Free Breathing Cardiac Perfusion MRI Reconstruction using a sparse and low rank model: Validation with the Physiologically Improved *NCAT* phantom

Sajan Goud, *Student Member, IEEE* and Mathews Jacob *Member, IEEE*

***Abstract*—We recently proposed an accelerated dynamic magnetic resonance imaging (MRI) reconstruction algorithm that exploits the underlying low rank and sparse properties of the data to achieve highly accelerated reconstructions. In this paper, we validate our algorithm in the context of dynamic free breathing cardiac Perfusion MRI on the Physiologically Improved Non Uniform Cardiac Torso Phantom, PINCAT phantom. The practical utilities of our scheme in providing significantly better reconstructions at higher accelerations in comparison to existing methods are studied. We demonstrate that our scheme donot have trade offs with accurate temporal modeling and spatial quality unlike the existing low rank based schemes. Our results also show the capability of our scheme to achieve better reconstruction qualities at high accelerations in comparison to using only the low rank or sparsity properties individually. We argue that the speed up obtained by our scheme could be capitalized in perfusion imaging to provide better spatio-temporal resolutions and volume coverage while the subject is freely breathing**

I. Introduction

Over the recent past, dynamic contrast enhanced cardiac perfusion MRI has become a useful tool to detect the presence of coronary artery disease. This involves the acquisition of temporal cardiac images that capture the uptake and wash out of the contrast agent through different regions of the heart. For an accurate clinical perfusion quantification study, the following inter dependent demands have to be met: (a) high temporal resolution (1-2 heartbeats) and long breath-hold duration (35-50 seconds) to accurately fit the kinetic model (b) good in-plane spatial resolution ($\leq 3mm^2$) to detect sub endocardial ischemia, assess transmural extent of defects, and minimize dark-rim artifacts, and (c) good spatial coverage ($\approx$ 6-8 slices) to cover the entire heart. Since MRI is a slow acquisition technique, acquiring the full *k*-space data at every time frame would mean a significant compromise in the temporal resolution and volume coverage. To overcome this, the goal over the recent past has been to develop accelerated reconstruction schemes that could recover the underlying dynamic scene from under-sampled *k-t* space measurements.

The well known cardiac MRI accelerated techniques such as DIME, UNFOLD, k-t BLAST [1], [2], [3] are limited to applications where the signal of interest is approximately periodic such as in cine imaging; they specifically rely on compactly representing the signal in the *x-f* space; (*f*- temporal frequency). The *x-f* space is significantly disturbed and is no longer compact in the presence of the contrast agent and the breathing motion (which could result if the patient do not meet the long breath hold demands or in free breathing studies). The use of the Karhunen Loueve Transform (KLT) in representing a variety of dynamic signals has been gaining popularity due to its potential to compactly represent the signal, without making any assumptions on the periodicity of the signal [4], [5]. Liang introduced this in the context of Cardiac MRI, where he stacked the voxel time series row wise in a signal matrix. The linear dependency of the rows in this matrix (i.e, a low rank matrix) is equivalent to the signal being compact in the KLT space. The KLT coefficients in the *x*-KLT space are directly derived from the data and this representation is guaranteed to be compact, making it a promising tool for accelerated perfusion imaging. The use of the total variation (TV) penalty in constraining the spatial and temporal finite differences in the context of cardiac perfusion imaging has been studied by [6], [7]. While their scheme solves the aliasing problem efficiently at low accelerations, it tends to over-smooth some of the spatial features at higher accelerations.

We recently have proposed a spectrally regularized matrix recovery frame work that capitalizes both on the low rank and the sparsity properties of the signal to recover high quality reconstructions from highly sparse *k-t* samples (*k-t* SLR) [8]. *k-t* SLR brings in the following novel aspects that could benefit the acquisition scheme in a range of dynamic imaging applications:

- Simultaneous estimation of the temporal bases and spatial weights directly from the under-sampled *k-t* measurements as opposed to the conventional two step KLT based scheme of first estimating the temporal bases from training data and then the spatial weights from the sparse outer *k* space samples.
- Capability to incorporate flexible non Cartesian sampling trajectories as opposed to the rigid dual Cartesian sampling patterns used in conventional KLT schemes.
- Exploitation of the sparsity penalty in appropriate domains in conjunction with the low rank property, which could allow for efficient operations at higher accelerations.

In this paper, we study the utility of *k-t* SLR on first pass cardiac perfusion imaging by using the Physiologically Improved Non Uniform Cardiac Torso Phantom (PINCAT) [9]. We first review the *k-t* SLR scheme and then focus on validating the different novel aspects listed above.

II. *k-t* SLR: Formulating the Objective Function

For simplicity, we demonstrate the reconstruction of a 2D cardiac slice. The extension to 3D imaging is straightforward. We denote the spatio-temporal signal as $\gamma(\mathbf{x}, t)$, where $\mathbf{x}$ is the spatial location and t denotes time. The dynamic MRI measurements correspond to the samples of the signal in $k-t$

Sajan Goud and Mathews Jacob are with the Department of Biomedical Engineering, University of Rochester, NY, USA. e-mail: (see http://www.cbig.rochester.edu)

This work is supported by NSF award CCF-0844812.

space, corrupted by noise:

$$\mathbf{b}_i \quad = \quad \int_{\mathbf{x}} \gamma(\mathbf{x}, t_i) \exp\left(-j\mathbf{k}_i^T\mathbf{x}\right) d\mathbf{x} + \mathbf{n}_i; \quad i = 0, .., s-1.$$

Here, $(\mathbf{k}_i, t_i)$ indicates the i^{th} sampling location. We denote the set of sampling locations as $\Xi = \{(\mathbf{k}_i, t_i), i = 0, .., s-1\}$. The above expression can be rewritten in the vector form as $\mathbf{b} = \mathcal{A}(\gamma) + \mathbf{n}$, where, $\mathcal{A}$ is the Fourier sampling operator. The goal is to recover the signal $\gamma(\mathbf{x}, t)$ from the measured *k-t* space samples.

In dynamic imaging applications, the temporal profiles of the voxels, indicated by the n-dimensional vectors

$$\mathbf{q}_i = [\gamma(\mathbf{x}_i, t_0), \gamma(\mathbf{x}_i, t_1), .., \gamma(\mathbf{x}_i, t_{n-1})]^T; \\ i = 0, .., m-1, (m : \#ofvoxels)$$

are highly correlated or linearly dependent. Liang et. al., proposed to re-arrange the spatio-temporal signal $\gamma(\mathbf{x}, t)$ in a matrix form to exploit the correlations [**?**], [4]:

$$\mathbf{\Gamma} = \begin{bmatrix} \gamma(\mathbf{x}_0, t_0) & \dots & \gamma(\mathbf{x}_0, t_{n-1}) \\ \vdots & & \\ \gamma(\mathbf{x}_{m-1}, t_0) & \dots & \gamma(\mathbf{x}_{m-1}, t_{n-1}) \end{bmatrix} \tag{1}$$

The rows of $\mathbf{\Gamma}$ correspond to the voxels, while the columns represent the temporal samples. Since the rows of this $m \times n$ matrix are linearly dependent, the rank of $\mathbf{\Gamma}$, is given by $r < \min(m, n)$. An arbitrary $m \times n$ matrix of rank r can be decomposed as

$$\mathbf{\Gamma} = \underbrace{\mathbf{U}}_{m\times r}\underbrace{\mathbf{\Sigma}}_{r\times r}\underbrace{\mathbf{V}^H}_{r\times n} \tag{2}$$

This decomposition implies that the spatio-temporal signal $\gamma(\mathbf{x}, t)$ can be expressed as a weighted linear combination of r temporal basis functions [4]:

$$\gamma(\mathbf{x}, t) = \sum_{i=0}^{r-1} \rho_i(\mathbf{x})\, v_i(t). \tag{3}$$

The temporal basis functions $v_i(t)$ are the columns of the matrix $\mathbf{V}$ in (2) while the spatial weights $\rho_i(\mathbf{x})$ are the row vectors of $\mathbf{U\Sigma}$ (often termed as spatial weights).

We formulate the recovery of the signal matrix $\mathbf{\Gamma}$ problem as

$$\mathbf{\Gamma}^* \quad = \quad \arg\min_{\mathbf{\Gamma}} \|\mathcal{A}(\mathbf{\Gamma}) - \mathbf{b}\|^2 \\ \text{s.t } \left\{\text{rank}(\mathbf{\Gamma}) \leq \text{r}, \|\mathbf{\Phi}^{\text{H}}\mathbf{\Gamma}\mathbf{\Psi}\|_{\ell_0} < \text{K}\right\} \tag{4}$$

where the low rank property is exploited by the rank constraint and the sparsity by the $\mathbf{\Phi}$ and $\mathbf{\Psi}$ operators or transforms that sparsify the row space and column space of $\mathbf{\Gamma}$ respectively. The use of additional transforms to achieve the sparsity constraint allows one to reduce the degrees of freedom (dof) significantly; from $r(m + n - r)$ to $r(k_1 + k_2 - r)$, where $k_1 << m$ and $k_2 << n$ are the sparsity levels of the left and right singular vectors respectively. This property can reduce the measurements significantly to recover the matrix $\mathbf{\Gamma}$.

Rewriting the above constrained optimization problem using Lagrange's multipliers and relaxing the penalties, we obtain

$$\mathbf{\Gamma}^* = \arg\min_{\mathbf{\Gamma}} \|\mathcal{A}(\mathbf{\Gamma}) - \mathbf{b}\|^2 + \lambda_1\, \varphi(\mathbf{\Gamma}) + \lambda_2\, \psi(\mathbf{\Gamma}), \tag{5}$$

where $\varphi(\mathbf{\Gamma})$ is an appropriate spectral penalty that penalizes the singular values of the matrix and is a surrogate for the rank of the matrix. We use the general class of Schatten p-functionals, specified by

$$\varphi(\mathbf{\Gamma}) = (\|\mathbf{\Gamma}\|_p)^p = \sum_{i=1}^{\min\{m,n\}} \sigma_i^p \tag{6}$$

The above spectral penalty simplifies to the nuclear norm for $p = 1$. When $p \leq 1$, this penalty ceases to be a norm and is non-convex. In our studies, we use $p = 0.1$ due to its superior performance in suprressing singular values associated with artifacts when compared to using nuclear norm. The use of similar non-convex semi-norms are well-studied in the context of vector recovery and are found to significantly improve the reconstruction of the signal from fewer measurements in comparison to the standard ℓ_1 semi-norms [10]–[12].

$\psi(\mathbf{\Gamma}) = \|\mathbf{\Phi}^H\mathbf{\Gamma}\mathbf{\Psi}\|_{\ell_1}$ is a surrogate for the ℓ_0 term in the sparsity constraint of (4). We use the total variation (TV) norm to exploit the sparsity of the gradient of the entire volume. Specifically the TV norm of the entire volume is specified by

$$\psi(\mathbf{\Gamma}) = \left\| \sqrt{\sum_{i=0}^{2} \left|\mathbf{\Phi}_i^H\mathbf{\Gamma}\mathbf{\Psi}_i\right|^2} \right\|_{\ell_1} \tag{7}$$

where $\mathbf{\Phi}_0 = \mathbf{D}_x; \mathbf{\Psi}_0 = \mathbf{I}$, $\mathbf{\Phi}_1 = \mathbf{D}_y; \mathbf{\Psi}_1 = \mathbf{I}$, and $\mathbf{\Phi}_2 = \mathbf{I}; \mathbf{\Psi}_2 = \mathbf{D}_t$; $\mathbf{D}_x$, $\mathbf{D}_y$ and $\mathbf{D}_t$ are the finite difference matrices along x, y, and t respectively.

III. The Optimization Algorithm

We use a variable splitting algorithm to solve (5). Auxiliary variables ($\mathbf{R}$ and $\mathbf{S}_i$) are introduced to convert the unconstrained minimization problem in (5) to a simpler constrained one as follows:

$$\mathbf{\Gamma}^* \quad = \quad \arg\min_{\mathbf{\Gamma},\mathbf{R},\mathbf{S}} \|\mathcal{A}(\mathbf{\Gamma}) - \mathbf{b}\|^2 + \lambda_1\, \varphi(\mathbf{R}) + \lambda_2 \left\| \sqrt{\sum_{i=0}^{2} \|\mathbf{S}_i\|^2} \right\|_{\ell_1} \\ \text{s.t. } \mathbf{\Gamma} = \mathbf{R}; \;\; \mathbf{S}_i = \mathbf{\Phi}_i^H\mathbf{\Gamma}\mathbf{\Psi}_i; \; i = 0, 1, 2 \tag{8}$$

We now use the penalty method to solve (8), where we minimize:

$$\mathcal{D}_{\beta_1,\beta_2}(\mathbf{\Gamma}, \mathbf{R}, \mathbf{S}_i) = \|\mathcal{A}(\mathbf{\Gamma}) - \mathbf{b}\|^2 + \lambda_1\, \varphi(\mathbf{R}) + \lambda_2 \left\| \sqrt{\sum_{i=0}^{2} \|\mathbf{S}_i\|^2} \right\|_{\ell_1} \\ + \frac{\beta_1}{2}\|\mathbf{\Gamma} - \mathbf{R}\|^2 + \frac{\beta_2}{2}\sum_{i=0}^{2} \|\mathbf{\Phi}_i^H\mathbf{\Gamma}\mathbf{\Psi}_i - \mathbf{S}_i\|^2 \tag{9}$$

This expression has to be minimized with respect to $\mathbf{\Gamma}$, $\mathbf{R}$, and $\mathbf{S}_i; i = 0, 1, 2$ to solve (5). The second row of (9) are the penalties introduced to enforce the constraints $\mathbf{\Gamma} = \mathbf{R}$ and $\mathbf{S}_i = \mathbf{\Phi}_i^H\mathbf{\Gamma}\mathbf{\Psi}_i; i = 0, 1, 2$. We solve this joint penalty using a three step alternating minimization scheme, where we solve for a variable of interest assuming the other two to be fixed

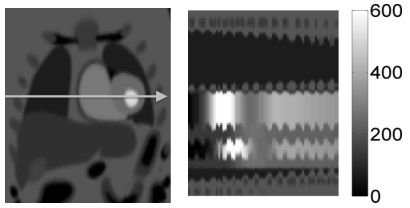

(a) A spatial frame (b) Temporal profile

Fig. 1. The PINCAT phantom used to validate the proposed scheme. A spatial frame at peak LV uptake along with the image time series through the arrow in (a) is shown in (b).

as follows:

$$\mathbf{\Gamma}_{n+1} = \arg\min_{\mathbf{\Gamma}} \|\mathcal{A}(\mathbf{\Gamma}) - \mathbf{b}\|^2 + \frac{\beta_1}{2}\|\mathbf{\Gamma} - (\mathbf{R}_n)\|^2 + \frac{\beta_2}{2}\sum_{i=0}^{2}\|\mathbf{\Phi}_i^H\mathbf{\Gamma}\mathbf{\Psi}_i - (\mathbf{S}_{i,n})\|^2, \quad (10)$$

$$\mathbf{R}_{n+1} = \arg\min_{\mathbf{R}} \|\mathbf{\Gamma}_{n+1} - \mathbf{R}\|^2 + 2\lambda_1/\beta_1\,\varphi(\mathbf{R}), \quad (11)$$

$$\mathbf{S}_{i,n+1} = \arg\min_{\{\mathbf{S}_i\}} \sum_{i=0}^{2}\|\mathbf{\Phi}_i^H\mathbf{\Gamma}_{n+1}\mathbf{\Psi} - \mathbf{S}_i\|^2 + 2\lambda_2/\beta_2 \left\|\sqrt{\sum_{i=0}^{2}\|\mathbf{S}_i\|^2}\right\|_{\ell_1}; i = 0,1,2 \quad (12)$$

We use a few Conjugate Gradient steps to obtain $\mathbf{\Gamma}_{n+1}$ by minimizing the quadratic cost function (10). (11) is solved as the singular value shrinkage:

$$\mathbf{R}^* = \sum_{i=0}^{\min(m,n)} \left(\sigma_i - \lambda\,\sigma_i^{p-1}/\beta\right)_+ \mathbf{u}_i\mathbf{v}_i^*, \quad (13)$$

Here, the shrinkage operator + is defined as:

$$(X)_+ = \begin{cases} X & \text{if} \quad X \geq 0 \\ 0 & \text{else} \end{cases} \quad (14)$$

The solution of (12) requires the joint processing of all the terms $\mathbf{P}_i; i = 0,1,2$, such that the magnitude $\sum_{i=0}^{2}\|\mathbf{P}_i\|^2$, is shrunk:

$$\mathbf{S}_{i,n+1} = \frac{\mathbf{P}_i}{\sum_{i=0}^{2}\|\mathbf{P}_i\|^2} \cdot \left(\sum_{i=0}^{2}\|\mathbf{P}_i\|^2 - \frac{\lambda_2}{\beta_2}\right)_+, \quad (15)$$

where $\mathbf{P}_i = \mathbf{\Phi}_i^H\mathbf{\Gamma}_{n+1}\mathbf{\Psi}$. This approach is termed as multidimensional shrinkage of $\{\mathbf{P}_i, i = 0,1,2\}$ [13].

High values of β_1 and β_2 are required for the constraints in (8) to hold, but this would result in slow convergence rate. On the other hand with low values of β_1 and β_2, one can increase the rate of convergence but would result in poor accuracy. To obtain a good tradeoff, we propose to solve a sequence of subproblems $\mathcal{D}_{\beta_1,\beta_2}$ with gradually increasing β_1 and β_2. This approach is observed to significantly improve the convergence rate, while maintaining the desired accuracy levels. To sum up, the alternating frame work starts with small values of β_1 and β_2, solves (9) by minimizing $\mathbf{\Gamma}$, $\mathbf{R}$, $\mathbf{S}_i$ i.e, (10), (11), (12) respectively in an alternating manner until convergence is met; (We term this as the inner loop). Next, the parameters β_1 and β_2 are updated in an outer loop to a higher number and the inner loop is again iterated. The outer loop is repeated until the conditions $\mathbf{R} \approx \mathbf{\Gamma}$ and $\mathbf{S}_i \approx \mathbf{\Phi}_i^H\mathbf{\Gamma}\mathbf{\Psi}_i;\ i = 0,1,2$ are achieved.

IV. Performance Evaluation

A. The PINCAT Phantom

To validate *k-t* SLR in the context of cardiac perfusion imaging, we use the Physiologically Improved Non uniform CArdiac Torso (PINCAT) numerical phantom [9]. The PINCAT phantom provides a realistic model of the dynamics of the different organs in the body. We focus on a single slice of the phantom, which has the cross section of the heart and consider dynamic contrast enhanced images with a temporal resolution of one heart-beat, acquired during the diastolic phase (where motion due to cardiac pumping is minimal). The time series data consists of 70 time frames corresponding to 70 heart-beats with respiratory motion (no breath-holding). The contrast variations due to bolus passage were modeled realistically in regions of the Right Ventricle, Left Ventricle and the Left Ventricle myocardium. The spatial matrix size is 128 x 128, which corresponds to a spatial resolution of 1.5 x1.5 mm^2. A spatial frame and the image time series of this data are illustrated in figure 1.

B. Methods

We test the proposed frame work against the following methods:

- Conventional KLT schemes [4], [5] with different sizes of training data (N_t)
- *k-t* FOCUSS [14], which relies on the sparsity of the signal in the *x-f* space
- Own variants of *k-t* SLR: Regularized schemes that relies on using only (a) Low rank or (b) sparsity properties

The reconstructions are evaluated at different accelerations (R), which is defined as the ratio of the number of acquired phase encodes in the fully sampled set to the number of phase encodes used to reconstruct the data. We quantify the performance of the algorithms using the signal to error ratio (SER) specified as

$$\text{SER} = -10\log_{10}\frac{\|\mathbf{\Gamma}_{\text{rec}} - \mathbf{\Gamma}_{\text{orig}}\|_F^2}{\|\mathbf{\Gamma}_{\text{orig}}\|_F^2}, \quad (16)$$

where $\|\cdot\|_F$ is the Frobenius norm.

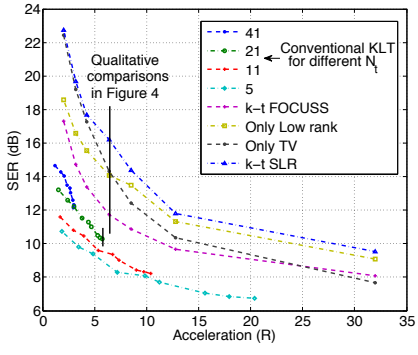

Fig. 2. SER in dB at different accelerations: Note that the k-t SLR scheme provides an improvement of 3-5 dB over k-t FOCUSS and conventional KLT based schemes and about 2dB over its own variants (low rank and TV penalties). The improvement over TV gets significant at higher Rs>5. The vertical black line at $R = 6.4$ points to specific qualitative comparisons in figure 4.

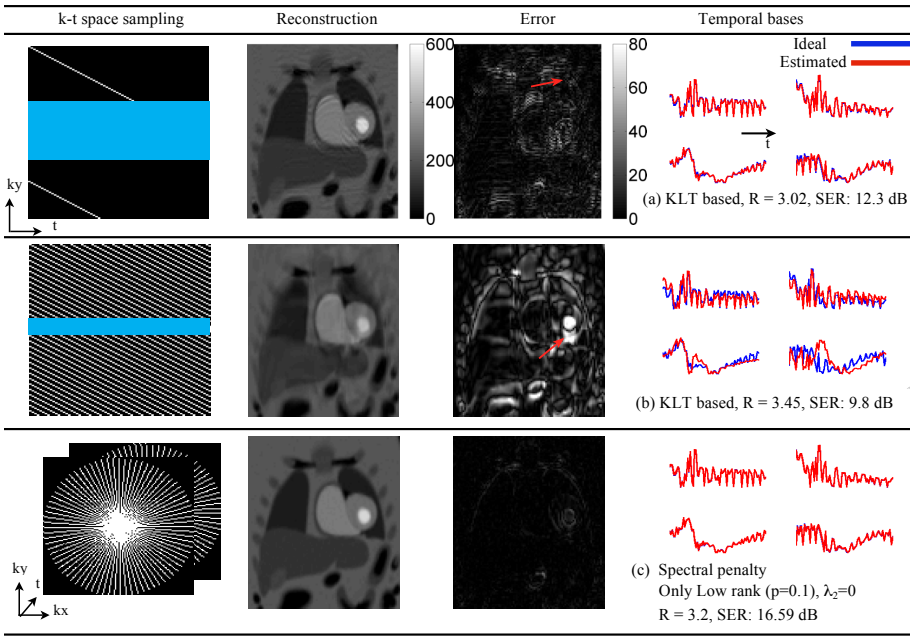

Fig. 3. Comparison of the standard KLT schemes with spectrally regularized reconstruction scheme; no sparsity priors are assumed in this comparison. Each row in the figure corresponds to the reconstructions with different reconstruction schemes and sampling patterns. We show the sampling pattern, a frame of the reconstructed dataset, the corresponding error image (shown at the same scale in all the insets), and the estimated temporal basis functions ($v_i(t)$, $i = 2$ to 5) overlaid on the actual temporal basis functions in each row. It is seen that the classical KLT based schemes experience a tradeoff between spatial aliasing and accuracy of temporal modeling. The first row correspond to classical KLT schemes with $Nt = 41$, where the basis functions are estimated correctly. However, the sparse sampling of outer k-space regions results in spatial aliasing. The temporal basis functions fail to capture the dynamics, when the number of phase encodes in training data is reduced to $Nt = 5$ in the second row; it is seen that the movement of the heart due to respiration is modeled inaccurately (pointed by the arrow). The spectrally regularized reconstruction scheme is capable of accurately estimating the temporal bases and spatial weights directly from the undersampled data. The use of a flexible radial sampling pattern also enables the spectrally regularized scheme to spread the alias patterns in an in-coherent manner.

We add zero mean Gaussian random noise to the *k-t* measurements such that the signal to noise ratio is 46 dB. For the Classical KLT schemes which assume a dual density Cartesian sampling pattern (see figure 3 for the sampling trajectory used), we assume the number of principal components to be 20. The remaining schemes (k-t FOCUSS, k-t SLR and its variants (low rank constraint alone, TV constraint alone) are capable of accounting for arbitrary non-Cartesian sampling patterns. For these schemes, we consider a radial trajectory with uniform angular spacing; the angular spacing between the spokes is chosen to obtain the specified *R*. The trajectory is rotated by a random angle in each temporal frame to make the measurements incoherent. We use the NUFFT approximation [15] to realize the $\mathcal{A}$ operator. See Figure 3 for an illustration. We choose the regularization parameters λ_1 & λ_2 for all the regularized schemes (k-t FOCUSS, k-t SLR, low rank penalty alone, and TV penalty alone) such that the SER of the reconstructions are maximized. We compare the reconstructions with the known ground truth for these comparisons. All of the regularized schemes are initialized with the zero filled IFFT reconstruction/gridding and iterated until convergence.

C. Validation

We initially demonstrate the utility of the proposed spectrally regularized matrix recovery frame work to recover low rank matrices effectively in comparison to conventional KLT schemes in figure 3. No sparsity priors are used in our scheme since the focus is to evaluate the performance in recovering low rank matrices. We observe that the accuracy of the temporal basis functions estimated with the classical schemes is dependent on the number of central phase encodes in the training data; theres a trade off in the estimation quality of the temporal bases and spatial reconstructions with the classical KLT scheme. Since the spectrally regularized matrix recovery scheme estimates the temporal bases and the spatial weights directly from the under-sampled data, the estimates are more representative of the data and hence accurate. The advantage of employing a flexible non Cartesian sampling pattern is also exploited by the use of the proposed scheme.

We next show the quantitative comparisons of all the schemes at different *R*s in figure 2. We observe that *k-t* SLR has a consistent 3-5 dB improvement in SER over Conventional KLT and *k-t* FOCUSS schemes. The improvement over using only low rank and only TV penalties are also significant (about 2 dB). In general we observe, using low rank property alone has residual aliasing and temporal over smoothing while using TV alone tends to over-smooth the spatial features significantly at higher *R*s (> 5). Conventional KLT schemes have the tradeoff between temporal modeling and spatial quality as discussed above. k-t FOCUSS has significant motion artifacts, since the sparsity of the x-f space is significantly disturbed with the perfusion and breathing changes. We demonstrate these behaviors qualitatively in figure 4 at $R \approx 6$. From this figure, we show that at high *Rs* > 5, where all the other schemes have compromises in their reconstructions, *k-t* SLR

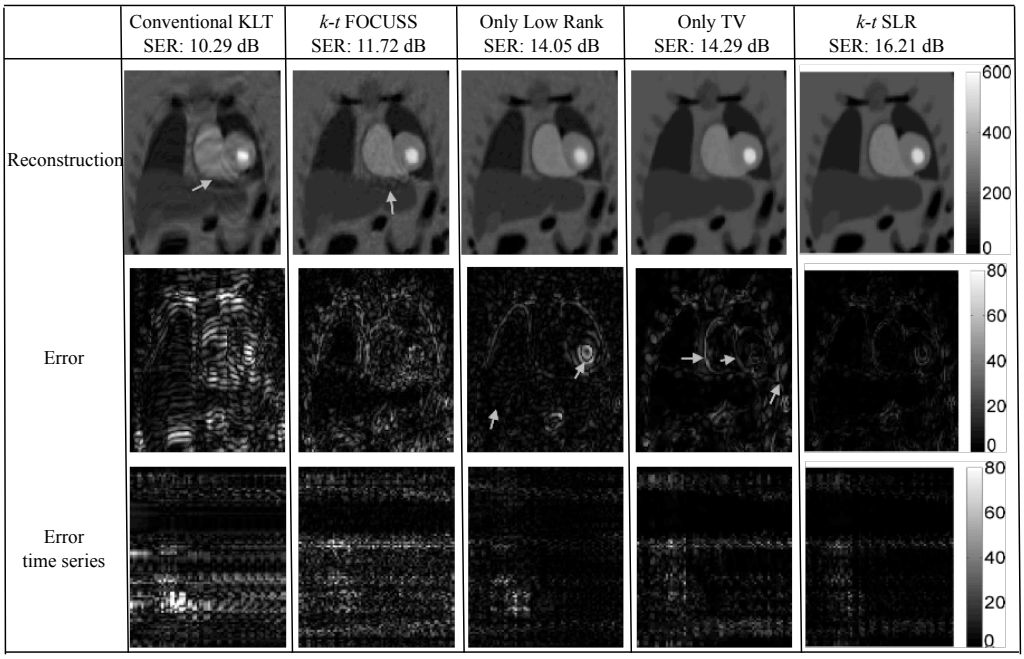

Fig. 4. Performance evaluation of k-t SLR in comparison with different schemes at $R \approx 6$: The Conventional KLT scheme is shown at $R = 5.74$ while the others are shown at $R = 6.4$. The conventional KLT scheme exhibit incorrect temporal modeling and spatial aliasing .Since k-t FOCUSS rely on the sparsity in the $x - f$ space, which is disturbed in the presence of breathing motion, inter frame motion artifacts manifests in its reconstructions(arrow in the inset of k-t FOCUSS reconstruction). In the spectrally regularized schemes, the use of the low rank constraint alone tend to penalize the singular values excessively, resulting in temporal smoothing. The low rank constraint alone does not get rid of the spatial artifacts completely resulting in residual streaking artifacts (arrows in the low rank insets). The use of the TV scheme alone tends to lose some important details due to over spatial smoothening (arrows in TV insets). For instance, the border between the left ventricular myocardium and the right ventricular blood pool is lost completely and the border between the right ventricular blood pool and the right ventricular myocardium is smeared (arrows in TV insets). It is observed that the k-t SLR combines the advantages of both low rank and TV schemes to provide more accurate reconstructions

recovers the underlying dynamic perfusion scene efficiently making it a useful tool for perfusion imaging aiming at high spatio-temporal resolutions, better volume coverage while the subject is freely breathing.

V. Conclusions

We validated the practical utilities of the *k-t* SLR algorithm in the context of free breathing perfusion imaging. In particular, we showed improvised reconstructions against conventional KLT schemes which have compromises between the spatial quality and accurate temporal modeling. The utility of the joint low rank and TV penalty allowed for exploiting the inherent redundancy of the data effectively and allowed for operations at higher accelerations ($R > 5$). With cardiac perfusion MR imaging having contradicting demands in achieving better spatio-temporal resolutions, minimal breath hold constraints, larger volume coverage, the efficient accelerated reconstructions provided by *k-t* SLR could bring in a potential practical advantage. The current work thats on progress is on further validating the *k-t* SLR scheme on in-vivo data sets with consideration to further speed ups by techniques such as Parallel Imaging.

References

[1] Z. Liang, H. Jiang, C. Hess, and P. Lauterbur, "Dynamic imaging by model estimation," *International Journal of Imaging Systems and Technology*, vol. 8, no. 6, pp. 551–557, 1997.

[2] B. Madore, "Using UNFOLD to remove artifacts in parallel imaging and in partial-Fourier imaging," *Magn Reson Med*, vol. 48, no. 3, pp. 493–501, Sep 2002.

[3] J. Tsao, P. Boesiger, and K. Pruessmann, "kt BLAST and kt SENSE: dynamic MRI with high frame rate exploiting spatiotemporal correlations," *Magnetic Resonance in Medicine*, vol. 50, no. 5, pp. 1031–1042, 2003.

[4] Z. Liang, "Spatiotemporal imaging with partially separable functions," in *ISBI*, 2007, pp. 181–182.

[5] H. Pedersen, S. Kozerke, S. Ringgaard, K. Nehrke, and W. Y. Kim, "k-t PCA: temporally constrained k-t BLAST reconstruction using principal component analysis," *Magn Reson Med*, vol. 62, no. 3, pp. 706–716, Sep 2009.

[6] G. Adluru, R. Whitaker, and E. DiBella, "Spatio-temporal constrained reconstruction of sparse dynamic contrast enhanced radial MRI data," in *4th IEEE International Symposium on Biomedical Imaging*, 2007, pp. 109–112.

[7] G. Adluru, C. McGann, P. Speier, E. Kholmovski, A. Shaaban, and E. DiBella, "Acquisition and reconstruction of undersampled radial data for myocardial perfusion magnetic resonance imaging," *Journal of Magnetic Resonance Imaging*, vol. 29, no. 2, pp. 466–473, 2009.

[8] S. Goud, Y. Hu, and M. Jacob, "Real-time cardiac MRI using low-rank and sparsity penalties," in *Proceedings of the ISBI, 2010*.

[9] B. Sharif and Y. Bresler, "Physiologically improved ncat phantom (pincat) enables in-silico study of the effects of beat-to-beat variability on cardiac mr," in *Proc. 15th Intl. Soc. Mag. Reson. Med. (ISMRM)*, 2007, p. 3418.

[10] J. Trzasko and A. Manduca, "Relaxed conditions for sparse signal recovery with general concave priors," *IEEE Trans. SP*, vol. 57, no. 11, pp. 4347–4354, 2009.

[11] I. Gorodnitsky and B. Rao, "Sparse signal reconstruction from limited data using focuss: A re-weighted minimum norm algorithm," *IEEE Transactions on Signal Processing*, vol. 45, no. 3, 1997.

[12] R. Chartrand, "Exact reconstruction of sparse signals via nonconvex minimization," *IEEE Signal Processing Letters*, vol. 14, no. 10, pp. 707–710, 2007.

[13] J. Yang, Y. Zhang, and W. Yin, "A fast TVL1-L2 minimization algorithm for signal reconstruction from partial Fourier data," *IEEE J. Special Topics Signal Processing, to appear*.

[14] H. Jung, J. Park, J. Yoo, and J. C. Ye, "Radial k-t FOCUSS for high-resolution cardiac cine MRI," *Magnetic Resonance in Medicine*, Oct 2009.

[15] M. Jacob, "Optimized least-square nonuniform fast fourier transform," *IEEE Transactions on Signal Processing*, vol. 57, no. 6, pp. 2165–2177, 2009.